Task-Invariant Passivity-Based Control of a Knee-Ankle Exoskeleton over the Primary Activities of Daily Life

Jianping Lin, Nikhil V. Divekar, Gray C. Thomas, *Member, IEEE*, Robert D. Gregg, *Senior Member, IEEE*

***Abstract*— State-of-the-art powered exoskeletons use trajectory-based, kinematic control methods for specific tasks. This type of control is appropriate for paraplegia, where the exoskeleton provides complete assistance. However, it overly constrains the volitional motion of people with remnant voluntary ability, e.g., stroke patients. In contrast, trajectory-free control methods are now being developed to provide task-invariant partial assistance for practicing/relearning leg motions or performing a continuum of activities in varying environments. Robotics systems like powered exoskeletons can be represented in the format of the Euler-Lagrange equation or the equivalent class, the port-controlled Hamiltonian equations. Our previous work proposed a novel optimal total energy shaping framework to alter the dynamical system's energy through the interconnection structure of a port-controlled Hamiltonian system model. The control law provides torques that depend on various basis functions related to gravitational and gyroscopic terms and produces able-bodied joint torques during walking on multiple ground slopes. In this paper, we extend the total energy shaping framework to provide flexible shaping structures with more freedom to change closed-loop dynamics. We enlarge the number of basis functions incorporating vertical ground reaction forces and global planar orientation to achieve better performance for assistance. We apply the framework to powered exoskeletons for optimal assistance across primary daily life activities and perform experiments on multiple human subjects to demonstrate the possible clinical benefits of optimal total energy shaping framework with powered lower-limb exoskeletons.**

I. Introduction

Powered exoskeletons, which arise from the development of the biped robot, have been widely studied with the potential use as a means of locomotion in rough terrain. Unlike the conventional orthotic devices, which are mechanically passive mechanisms, powered exoskeletons can enhance a healthy person's abilities or support a physically impaired person's activities of daily living by providing powered hip, knee, or ankle motions based on different control designs. Researchers proposed many different methods for the controller design of these rehabilitation devices. State-of-the-art powered exoskeletons are mainly controlled by tracking pre-defined reference trajectories. For instance, ReWalk [1], and Ekso Bionics [2] applied the control technology with pre-defined reference trajectories determined by a finite-state machine. The controller of the robot suit, the Hybrid Assistive Limb [3], generates motion patterns for the assisted leg based on inter-limb locomotor synergies and kinesiological information. The bilateral Wandercraft exoskeleton [4] utilized the controller based on virtual constraints, hybrid zero dynamics, and gait optimization.

Despite the promising results in gait rehabilitation of powered exoskeletons, significant challenges remain in the control design. The state-of-the-art exoskeletons mentioned above provide complete assistance with trajectory-based, kinematic control methods appropriate for paraplegia. These kinematic control methods replicate the normative joint kinematics associated with one specific task and user at a time [5]. However, the control structures enforce trajectories defined in a database, which cannot adjust to undefined varying daily tasks. Thus, it cannot adjust to continuously varying activities and overly constrains the volitional motion of people with remnant voluntary ability, e.g., stroke patients. It introduces patient complacency and dramatically diminishes the stimulation and level of difficulty, ultimately reducing learning [6].

Moreover, these devices also have to detect human locomotor intention accurately to transition from one task-dependent controller to another [1], which is hard to realize in practice [7]. The associated parameter tuning for multiple controllers requires more time for each subject and task, and this procedure will continue as users make progress in gait training [8]. In addition, the stiff actuators associated with rigid position control enable large output torques for moving the user's legs with high-ratio transmissions, which come with a high mechanical impedance that prevents users from moving their joints freely without help from the exoskeleton [9].

Instead of providing complete assistance, partial assistance can provide backdrivability based on energetic control, enabling us to consider a paradigm shift from task-specific, kinematic control approaches to task-invariant, energetic control approaches. The trajectory-free control provides partial assistance while the user practices or relearns their leg motions. Backdrivability refers to the exoskeleton joints with low actuators' output impedance, which means users can drive their joints without a high resistive torque from the exoskeleton. This is a necessary requirement for assisting or augmenting volitional human motion and benefits the design of task-invariant control, which can provide flexibility in assisting humans in a continuum of activities despite the specific tasks and environment changes as mentioned in [10]. Various assistive controllers have been proposed for exoskeletons to amplify and augment human motion [11]–

This work was supported by the National Science Foundation under Award Number 1652514 / 1949869.

J. Lin, N. V. Divekar, G. C. Thomas, and R. D. Gregg are with the Department of Electrical Engineering and Computer Science and the Robotics Institute, University of Michigan, Ann Arbor, MI 48109, USA. (Correspondence: rdgregg@umich.edu)

[13], or compensate for exoskeleton mass/inertia [14], [15]. In [16], a lightweight hip exoskeleton with high backdrivability was designed to provide partial assistance. However, the controller detects gait intention and is still based on pre-defined trajectories. In [15], a trajectory-free assistive controller was proposed to provide a combination of body-weight compensation and stance stabilization through the hip and knee actuators. However, the controller focuses on reducing the joint-level gravitational torques instead of considering the lower-limb model of the whole walking system.

An energy shaping method can serve as the task-invariant control by altering the dynamic characteristics of the human body, which have already seen success in applications of powered exoskeletons with high backdrivability [17]. Energy shaping methods [18], [19] alter the dynamic characteristics of the human body via the Euler-Lagrange equations (or the Hamiltonian equations). The applications of the energy shaping methods satisfy the set of nonlinear partial differential equations (PDEs) corresponding to the *matching conditions*, which determine the achievable form of the closed-loop system's energy and dedicate the existence of a feedback law to match the original control system to the designed closed-loop system. With the obtained solution of the matching conditions, the feasible structure of the closed-loop system can be derived and provides flexibility to the design of suitable closed-loop Euler-Lagrange systems (or Hamiltonian systems).

In [20], [21], the proposed potential energy shaping control based on the controlled Lagrangian method provides virtual body-weight support (BWS) during the walking gait, where the compensation of the inertia forces/torques are not considered. Approaches have also been proposed to consider the total energy in [17], [22]–[24]. The total energy shaping (TES) method achieves further assistance during walking with modified mass/inertia matrices in addition to the modified potential energy for inertia compensation. However, the corresponding controller requires complicated calculations of the mass/inertia matrix inverse, where the computational cost of matrix inversion scales quadratically with matrix dimension [25]. The flexibility of finding the proper mass/inertia matrix to achieve positive definiteness also limits the overall performance of the proposed method in the real-time implementation of our powered knee-ankle orthosis (Fig. 1, left). The stability of the altered dynamical system is only considered during the fully-actuated phase (i.e., flat foot contact). During the underactuated phases (i.e., heel contact and toe contact), the closed-loop potential energy in [17], [22] cannot be retrieved directly from the altered dynamical system and can only be approximated due to the lack of an analytical expression.

In contrast to the TES method with modified mass/inertia matrix in [17], [22], we combined the modified closed-loop potential energy with the additional virtual spring and damping energy to propose the indirect TES method (i.e., indirect kinetic terms corresponding to the damping energy) [26]. The proposed method achieves passivity and stability during all contact conditions. Passivity is defined in [27], which guarantees the change of the system energy to be bounded by the energy injected through the input, i.e., the human controls the energy growth of the coupled human-exoskeleton system. Simultaneously, Lyapunov stability ensures the response will remain in a neighborhood of equilibrium under human impedance control. Despite the promising simulation results in [26], the range of the reasonable virtual spring stiffness and the passivity conditions limit the virtual spring and damping coefficients and the flexibility of the indirect kinetic terms, where significant results cannot be provided compared to the potential energy shaping method.

In [28], we derived a novel energetic control strategy based on the Interconnection and Damping Assignment Passivity-based Control (IDA-PBC) method [29], [30] for a backdrivable knee-ankle exoskeleton. We achieved an indirect-kinetic-energy shaping without modifying the mass/inertia matrix (avoiding matrix inversion in the matching condition) by modifying the interconnection structure. The control law provides torques that depend on various designed basis functions corresponding to gravitational force vectors and gyroscopic forces. The designed basis functions enable velocity-dependent assistance, e.g., during early and late stance, which was impossible in prior implementations of potential energy shaping. We performed a proof-of-concept experiment with an able-bodied human subject to demonstrate the proposed controller's ability to assist in multiple walking conditions, i.e., ramp incline/decline and level-ground walking. Despite the promising results in [28], there are still several limitations associated with the energetic control strategy.

As mentioned in [31], our model assumes the stance leg is fully loaded with the user's weight. This results in excessive plantar-flexion torques as weight transfers from the assisted leg to the contralateral leg during double support. This excessive plantar-flexion can aggravate the foot-drop problem later in swing, during both walking and stair climbing. As a result, we consider the effect of the ground reaction force (GRF) into the basis functions during the optimization process in this paper. Moreover, the modified gravitational vector in [28] depends only on the actuated variables. The corresponding potential energy shaping controller behaves as nonlinear springs, which does not consider the global variable (planar orientation of the system model) of the human-exoskeleton system, i.e., the gravity's direction. We consider the global variable in this new approach of potential energy shaping and investigate the input-output passivity and stability of the human-exoskeleton system with a generally shaped structure in the closed-loop dynamics. This investigation extends the passivity proof in [23], [24] during the fully-actuated phase (i.e., flat foot contact) to the whole walking gait cycle. Incorporating the global variable increases the candidate basis functions in the optimization process, achieving an optimal controller that fits normative human joint torques more closely. As a result, we have more flexibility in designing the shaped closed-loop structure to achieve better performance for assistance.

Meanwhile, we consider "L1 regularization", which fits the data with as few parameters as possible to avoid overfit-

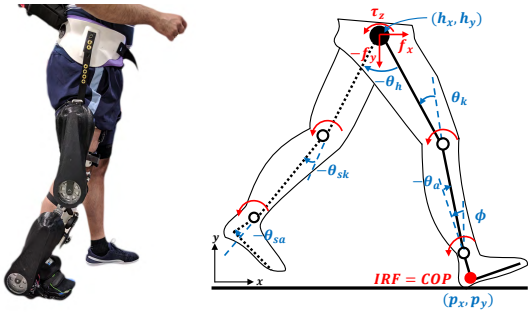

Fig. 1. Left: Comex knee-ankle exoskeleton worn by a healthy user (reproduced from [31]). Right: Kinematic model of the human body (reproduced from [26]). COP denotes Center of Pressure. The solid links denote the stance leg, and the dashed links denote the swing leg. Red arcs indicate torques.

ting problems. We formulate and solve the optimization problem using convex programming tools. The optimal controller is assessed in terms of the similarity and variance accounted for (VAF) to normative human torques in the simulation. We also extend the proposed TES framework with additional sit-stand cycle and stairs walking tasks, which are equally important activities of daily living. Improvements gained in walking ability do not necessarily transfer to stair climbing, and a lack of rehabilitation in sit-to-stand contributes to the increased fall risk in the post-stroke population [32], [33]. In the end, we perform experiments on multiple human subjects to demonstrate the possible clinical benefits of the optimal TES method with powered lower-limb exoskeletons.

The contributions are summarized as follows:

- We propose a new control law that provides torques based on a linear combination of designed basis functions with the global planar orientation variable and GRFs incorporated, which enables closer fitting to the normative human torques.
- We provide input-output passivity and stability with the incorporation of the additional global variable and formulating a TES framework with a more flexible shaping structure for controller design than the one in [28].
- We assess the muscular effort of multiple able-bodied human subjects with the first experimental implementation of TES on an exoskeleton considering primary activities of daily life, including level-ground, ramps, stairs walking, and sit-stand cycle.

II. Modeling and Control Methods

In this section, we briefly review interconnection and damping assignment passivity-based control (IDA-PBC) for the human-exoskeleton system [28]. We incorporate a global foot angle variable in the control law and prove input-output passivity and stability. We also provide an improved optimization process for matching normative human data with multiple tasks.

A. Review of the Human-Exoskeleton Dynamics

We consider a 6-link sagittal plane human-exoskeleton biped model with a floating stance foot and five revolute joints (Fig. 1). The Cartesian coordinates of the heel, (p_x, p_y), are defined with respect to the inertial reference frame (IRF). The global heel angle ϕ is defined with respect to the vertical axis. And θ_a and θ_k are the stance ankle and knee angles, respectively. The angle between the stance thigh and the swing thigh is denoted by θ_h and θ_{sk} and θ_{sa} are the swing knee and ankle angles, respectively. The masses in the model reflect the combination of the human and exoskeleton masses.

For control purposes, the dynamics of the stance and swing legs are modeled separately with coupled interaction forces $F = [f_x, f_y, \tau_z]^T$. The five degree-of-freedom (DOF) stance leg model has the generalized coordinates $q = [p_x, p_y, \phi, \theta_a, \theta_k]^T$ (solid in Fig. 1). The conjugate momenta $p = M(q)\dot{q}$ are defined by the positive-definite inertia matrix $M(q) \in \mathbb{R}^{5\times5}$ and the velocity vector $\dot{q}$. The port-controlled Hamiltonian dynamics can be characterized by the Hamiltonian $H(q,p) = \frac{1}{2}p^T M^{-1}(q)p + V(q)$, where $V(q)$ is the potential energy, as

$$\begin{bmatrix}\dot{q}\\ \dot{p}\end{bmatrix} = \begin{bmatrix}0_{5\times5} & I_{5\times5}\\ -I_{5\times5} & 0_{5\times5}\end{bmatrix}\nabla H + \begin{bmatrix}0_{5\times1}\\ \tau + A^T\lambda\end{bmatrix}, \tag{1}$$

where the gradient $\nabla H = [(\partial_q H)^T, (\partial_p H)^T]^T$, and the vector of joint torques $\tau \in \mathbb{R}^5$ aggregates the exoskeleton input $\tau_{\text{exo}} = Gu$ and the human input $\tau_{\text{hum}} = Gv + J(q)^T F$. The control inputs $u \in \mathbb{R}^2$ and $v \in \mathbb{R}^2$ represent the exoskeleton and human torques at the knee and ankle joints, respectively. They are mapped into the overall dynamics via matrix $G \in \mathbb{R}^{5\times2}$. The system is underactuated with the number of generalized coordinates larger than the number of control inputs. The interaction forces F are mapped into the system's dynamics by the Jacobian matrix $J(q)$. The Lagrange multiplier λ represents the ground reaction forces (GRFs) and is mapped into the system through the constraint matrix A. From now on we omit q and p terms in matrices to simplify notation.

Following [17], we incorporate holonomic contact constraints in the human-exoskeleton dynamics (Fig. 2). The constraint functions can be expressed as $a_\ell(q) = 0_{c\times1}$, where c is the number of constraints and the subscript $\ell \in \{\text{heel}, \text{flat}, \text{toe}\}$ indicates the contact configuration. The constraint matrix $A = \nabla_q a_\ell \in \mathbb{R}^{c\times5} = [A_\ell\ 0_{c\times2}]$ satisfies $A\dot{q} = A\partial_p H = 0$ given the top row of (1). The possible cases are

$$\begin{aligned}
\text{Heel Contact}\quad & a_{heel}(q) = (p_x, p_y)^T = 0_{2\times1},\\
& A_{heel}(q) = \begin{bmatrix}I_{2\times2} & 0_{2\times1}\end{bmatrix},\\
\text{Flat Foot}\quad & a_{flat}(q) = (p_x, p_y, \phi - \gamma)^T = 0_{3\times1},\\
& A_{flat}(q) = I_{3\times3}, \text{ and}\\
\text{Toe Contact}\quad & a_{toe}(q) = \begin{bmatrix}p_x - l_f(\cos\gamma - \cos\phi)\\ p_y - l_f(\sin\gamma - \sin\phi)\end{bmatrix} = 0_{2\times1},\\
& A_{toe}(q) = \begin{bmatrix}1 & 0 & -l_f\sin(\phi)\\ 0 & 1 & l_f\cos(\phi)\end{bmatrix},
\end{aligned}$$

where γ is the slope angle and l_f is the length of the foot. More details for the contact constraints are given in [17], [21].

For the swing leg model (dotted in Fig. 1), the configuration vector is given by $q_{sw} = [h_x, h_y, \theta_{th}, \theta_{sk}, \theta_{sa}]^T$, where

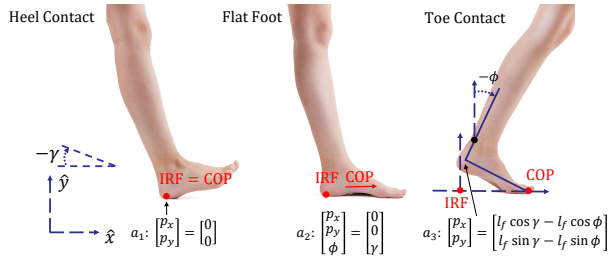

Fig. 2. Heel contact (left), flat foot (center), and toe contact (right) during the single-support period of human locomotion. The biped is assumed to be walking on a slope with angle γ. This figure is updated from [17].

(h_x, h_y) are the positions of the hip with respect to the IRF. The angle between the vertical axis and the swing thigh is denoted as θ_{th}. The swing leg dynamics do not have contact constraints.

B. Matching Condition with Constrained Dynamics

As shown in [28], we explicitly express the GRFs in the dynamics to obtain a system in the port-controlled Hamiltonian format [29], where

$$\begin{bmatrix}\dot{q}\\ \dot{p}\end{bmatrix} = \mathscr{J}\nabla H + \begin{bmatrix}0\\ G_\lambda(u+v)+J_\lambda^T F\end{bmatrix}. \tag{2}$$

The skew-symmetric matrix $\mathscr{J} = -\mathscr{J}^T$ is defined as

$$\mathscr{J} = \begin{bmatrix}0 & X_\lambda^T\\ -X_\lambda & Y_\lambda\end{bmatrix},\ X_\lambda = I - A^T W A \partial_{p^2}^2 H,$$
$$Y_\lambda = -A^T W \partial_q (A\partial_p H)^T + \partial_q (A\partial_p H) W A,$$

where $W = (A\partial_{p^2}^2 H A^T)^{-1} \in \mathbb{R}^{c\times c}$ and we apply $A\partial_p H = 0$ to obtain the upper-right block of the matrix $\mathscr{J}$. The matrix $\mathscr{J}$ reveals the internal interconnection structure of the open-loop dynamics, and matrices $G_\lambda = X_\lambda G$ and $J_\lambda^T = X_\lambda J^T$ are defined respectively.

Assume we have closed the feedback loop for exoskeleton input u, while the human inputs v and F remain open-loop in the Hamiltonian system. We consider a desired, closed-loop Hamiltonian $\tilde{H}(p,q) = \frac{1}{2}p^T\tilde{M}^{-1}p + \tilde{V}$, where $\tilde{V} = V + \hat{V}$ represents the new potential energy with shaping term $\hat{V}$. The corresponding gravitational vector is $\tilde{N} = \nabla_q \tilde{V} = \nabla_q V + \nabla_q \hat{V} = N + \hat{N}$. We set $\tilde{M} = M$ to simplify the matching process and avoid complicated calculations of the inverse of the mass/inertia matrix in the control law, where $\nabla\tilde{H} = \nabla H + [\nabla_q \hat{V}, 0]^T$. However, we can still achieve velocity-dependent shaping through the interconnection structure of the closed-loop Hamiltonian system.

The desired closed-loop dynamics based on $\tilde{H}$ are

$$\begin{bmatrix}\dot{q}\\ \dot{p}\end{bmatrix} = \begin{bmatrix}0 & I\\ -I & J_2\end{bmatrix}\nabla\tilde{H} + \begin{bmatrix}0\\ Gv + J^T F + A^T\tilde{\lambda}\end{bmatrix}, \tag{3}$$

where the skew-symmetric matrix J_2 represents the extra DOF provided by the IDA-PBC method, and

$$\tilde{\lambda} = (A\partial_{p^2}^2 H A^T)^{-1}\{-\partial_q(A\partial_p H)^T\partial_p H + A\partial_{p^2}^2 H[\partial_q\tilde{H} - J_2\partial_p H - Gv - J^T F]\}.$$

Plugging $\tilde{\lambda}$ into (3), we have

$$\begin{bmatrix}\dot{q}\\ \dot{p}\end{bmatrix} = \tilde{\mathscr{J}}\nabla\tilde{H} + \begin{bmatrix}0\\ G_{\tilde{\lambda}}v + J_{\tilde{\lambda}}^T F\end{bmatrix}, \tag{4}$$

where

$$\tilde{\mathscr{J}} = -\tilde{\mathscr{J}}^T = \begin{bmatrix}0 & X_{\tilde{\lambda}}^T\\ -X_{\tilde{\lambda}} & Y_{\tilde{\lambda}}\end{bmatrix},\ X_{\tilde{\lambda}} = X_\lambda,$$
$$\begin{aligned} Y_{\tilde{\lambda}} &= -Y_{\tilde{\lambda}}^T,\\ &= J_2 - A^T W[\partial_q(A\partial_p H)^T + A\partial_{p^2}^2 H J_2]\\ &\quad + [J_2^T\partial_{p^2}^2 H A^T + \partial_q(A\partial_p H)]WA. \end{aligned}$$

Matrices $G_{\tilde{\lambda}}$ and $J_{\tilde{\lambda}}$ are equivalent to G_λ and J_λ.

Based on standard results in [19], Hamiltonian systems (2) and (4) *match* if we have

$$\begin{aligned} G_\lambda u &= -X_\lambda(\partial_q\tilde{H} - \partial_q H) + (Y_{\tilde{\lambda}} - Y_\lambda)\partial_p H,\\ &= X_\lambda(-\partial_q\tilde{H} + \partial_q H + J_2\partial_p H), \end{aligned}$$

which yields the corresponding *matching condition* as

$$0 = G_\lambda^\perp X_\lambda(-\partial_q\tilde{H} + \partial_q H + J_2\partial_p H), \tag{5}$$

where $G_\lambda^\perp \in \mathbb{R}^{3\times 5}$ is the (full-rank) left annihilator of G_λ, i.e., $G_\lambda^\perp G_\lambda = 0$. To solve the matching condition (5), we decompose the mass/inertia matrix M into four sub-matrices as in [28]

$$M = \begin{bmatrix}M_1 & M_2\\ M_2^T & M_4\end{bmatrix},$$

where $M_1 \in \mathbb{R}^{3\times 3}$ and $M_4 \in \mathbb{R}^{2\times 2}$. Then we obtain

$$M^{-1} = \begin{bmatrix}\Delta^{-1} & -\Delta^{-1}M_2M_4^{-1}\\ -M_4^{-1}M_2^T\Delta^{-1} & M_4^{-1} + M_4^{-1}M_2^T\Delta^{-1}M_2M_4^{-1}\end{bmatrix},$$

where $\Delta = M_1 - M_2M_4^{-1}M_2^T$. The solution of the matching condition (5) is given as

$$\begin{aligned} 0 &= \begin{bmatrix}I_{3\times 3} - Z_\lambda & 0_{3\times 2}\end{bmatrix}[-\partial_q\tilde{H} + \partial_q H + J_2\partial_p H],\\ &= \begin{bmatrix}I_{3\times 3} - Z_\lambda & 0_{3\times 2}\end{bmatrix}[-\tilde{N} + N + J_2M^{-1}p], \end{aligned} \tag{6}$$

where $Z_\lambda = A_\ell^T W A_\ell \Delta^{-1}$ and $W = (A_\ell\Delta^{-1}A_\ell^T)^{-1}$. By zeroing the unactuated parts (first three elements) of $-\tilde{N} + N + J_2M^{-1}p$, the matching condition (5) is satisfied. More details can be found in [28].

C. Shaping Structure and Control Law

The control law with the feasible shaping structure is

$$\begin{aligned} u &= G^+(\partial_q H - \partial_q\tilde{H} + J_2M^{-1}p),\\ &= G^+(-\hat{N} + J_2M^{-1}p), \end{aligned} \tag{7}$$

with $G^+ = (G^TG)^{-1}G^T$ being the left pseudoinverse of G. The closed-loop system (4) is integrable with a well-defined potential energy if the shaping stucture satisfy Proposition 2.1 in [28]. Integrability guarantees that there exists an equivalent Lagrangian $\tilde{L}(q,\dot{q}) = \frac{1}{2}\dot{q}^T M\dot{q} + \dot{q}^T Q(q) - \tilde{V}$ to ensure passivity. The modified gravitational vector $\hat{N}$ satisfying Proposition 2.1 in [28] depends only on the actuated variables and behaves as nonlinear springs. Instead of restricting systems to be integrable with well-defined potential energy,

similar to [34], we treat $\hat{N}$ and $J_2M^{-1}p$ as some external forces in the closed-loop system satisfying (6), where velocity dependence is introduced via the conjugate momenta $p = M(q)\dot{q}$. We can then incorporate the global variable ϕ into $\hat{N}$ and $J_2M^{-1}p$. We demonstrate the corresponding input-output passivity and stability proof during the whole walking gait in Section II-D.

In [28], we formed multiple basis functions for the shaping terms in (7) and converted our controller design into an optimization process to fit the normative joint moment data in [35]. These basis functions aim to change the effect of these forces and capture the essential characteristics of walking. In this approach, we extend the optimization procedure to include stairs walking and stand-to-sit tasks in addition to the ramp and level-ground walking in [28]. The incorporation of the global variable ϕ increases the candidate basis functions in the optimization process. As a result, we consider "L1 regularization" as in [35]. Minimizing the L1 norm encourages sparsity in the residual [36]. In our case, this encourages a sparse set of basis functions, which fits the data with as few parameters as possible to avoid over-fitting problems.

We design $\hat{N} = -\alpha_1\xi_1 - \cdots - \alpha_i\xi_i$ and $J_2M^{-1}p = \alpha_{i+1}\xi_{i+1} + \cdots + \alpha_w\xi_w$ as linear combinations of the basis functions $\{\xi_1, \xi_2, \ldots, \xi_w\}$, where $\xi_i \in \mathbb{R}^{5\times 1}$ and w is the total number of basis functions. As mentioned in [31], the model (1) does not know the state of the contralateral leg and the energy shaping controller compensates for a fraction of the full body weight during stance, even when part of the body weight is supported by the other leg. These issues were solved by implementing a GRF-based torque tapering strategy with a scaling factor multiplying the exoskeleton torque commands during the stance phase in [31]. As a result, we incorporate the vertical GRF (vGRF, which is normalized to one at 100% body weight) into (7) and express the torque control input as

$$\begin{aligned} u &= B^+(-\hat{N} + J_2M^{-1}p) \\ &= B^+(\alpha_1\xi_1 + \alpha_2\xi_2 + \cdots + \alpha_w\xi_w)\cdot \text{vGRF} \\ &= \Phi(q,p)\alpha \cdot \text{vGRF}, \end{aligned} \tag{8}$$

where $B^+ = [0_{2\times 3}, I_{2\times 2}]$ for the stance leg model and $\Phi(q,p) \in \mathbb{R}^{2\times w}$. We optimize the constant coefficients α so the outputs of control law u best fit normative human joint torques y when inputting normative human kinematic trajectories.

The optimization problem is defined as

$$\begin{aligned} \arg\min_{\alpha} \sum_j \{ &[\text{vGRF}\cdot U(q_j,p_j,\alpha) - Y_j]^T \cdot W_j(U,Y_j) \\ &\cdot [\text{vGRF}\cdot U(q_j,p_j,\alpha) - Y_j] \\ &+ [U^{\%}(q_j,p_j,\alpha) - Y_j^{\%}]^T W_k [U^{\%}(q_j,p_j,\alpha) - Y_j^{\%}]\} \\ &+ U(q_0,p_0,\alpha)^T W_r U(q_0,p_0,\alpha) + \Lambda \|W_s\alpha\|_1, \end{aligned} \tag{9}$$

where the first part of the objective function corresponds to the least square error of the exoskeleton control inputs $U \in \mathbb{R}^{m\times 1}$ and the normative human joint torques $Y_j \in \mathbb{R}^{m\times 1}$ with the weighting matrix $W_j(U,Y_j)$ and the number of time samples m. The subscript j represents the number of different walking tasks, including level-ground, ramp, stairs walking, and stand-to-sit. The state vectors $q_j, p_j \in \mathbb{R}^{m\times 1}$ comprise samples over time for the given task j. The weighting matrix $W_j(U,Y_j)$ depends on the exoskeleton and human inputs (U,Y_j) and adjusts the weights according to $\text{sign}(U(i)\cdot Y_j(i))$, where $i \in \{1,\ldots,m\}$ represents the sample index. We enlarge the weights when $U(i)$ and $Y_j(i)$ have opposite signs to emphasize the importance of consistent torque during walking gait in the optimization process. The second part of the objective function with $U^{\%}$ and $Y^{\%}$ aims to minimize the difference between the control inputs and normative torques during the initial 15% and late 15% of stance phase with weighting matrix W_k, i.e., the early and late stance phases during the gait cycle, without the effect of ground reaction forces. This helps regulate the exoskeleton torques u at endpoints of the stance phase and minimize the dependence on vGRF for real-time implementation when the sensor returns inconsistent measurements of vGRF compared to simulation. We also include W_r with states $p = p_0 = 0$ and $q = q_0$ in the third part of the objective function, where q_0 is the state when $\phi, \theta_a = 0$ and θ_k is hyper-extended. Minimal torques should be provided for the knee with hyper-extension as safety guidance by optimization. Lastly, we apply L1 regularization to enforce sparsity in models and shrink the parameters α to zero, where Λ is the penalty term which determines how much to penalize the weights. The weighting matrix W_s adjusts the optimal parameters associated with the gyroscopic terms and modified potential energy. We use "`fmincon`" with sequential quadratic programming in MatLab to find the optimal solutions α^* in a fast and efficient way. As a result, the corresponding control law equals $u = \Phi(q,p)\alpha^* \cdot \text{vGRF} \cdot \text{LOA}\%$, which will be scaled down to a desired fraction of normative torque through LOA% (level-of-assistance percent).

D. Passivity and Stability

We now explore the input-output passivity and stability results of the exoskeleton-human system with global variable ϕ incorporated in the modified potential energy for the stance leg model, i.e., $\hat{V} = \hat{V}(\phi, \theta_a, \theta_k)$. We define $\hat{N}$ as follows

$$\hat{N} = [0,0,0,\hat{N}_4(\phi,\theta_a,\theta_k),\hat{N}_5(\phi,\theta_a,\theta_k)]^T,$$

where the terms in $\hat{N}$ are defined from

$$\begin{aligned} -\hat{F}(q) &= \nabla_q \hat{V} \\ &= [0,0,\hat{N}_3(\phi,\theta_a,\theta_k),\hat{N}_4(\phi,\theta_a,\theta_k),\hat{N}_5(\phi,\theta_a,\theta_k)]^T, \end{aligned}$$

which represents the conservative force vector along with the modified potential energy function $\hat{V}$. Vector $\hat{N}$ comprises only the actuated components in $-\hat{F}$, i.e., $\hat{N}_4$ and $\hat{N}_5$ correspond to the conservative force vector acting on the ankle and knee joints with actuators.

Proposition 2.1: Assume $\hat{V}$ is continuously differentiable with $\int_0^t \hat{N}_3(\phi,\theta_a,\theta_k)\dot{\phi}d\delta$ bounded over a finite time t, then the closed-loop system (3) is passive from the human input τ_{hum} to the output $\partial_p H$.

Proof: The modified gravitational vector $\hat{N}$ is not well-defined with a symmetric Jacobian matrix, i.e., $\frac{\partial \hat{N}_i}{\partial q_j} \neq \frac{\partial \hat{N}_j}{\partial q_i}$

for any $i, j \in \{1, \cdots, 5\}$. As a result, we cannot have a valid potential energy $\tilde{V}$ in the closed-loop system retrieved by the variable gradient method [27]. We choose the following function $E(q,p)$ as a storage function

$$E = H + \hat{V} - \int_0^t \hat{N}_3(\phi(\delta), \theta_a(\delta), \theta_k(\delta))\dot{\phi}(\delta)d\delta + E^0, \quad (10)$$

where E^0 is a constant such that E is positive semi-definite. We have the integral over a path C in configuration space Q as

$$\begin{aligned}\hat{V}(t) - \hat{V}(0) = & \int_0^t \dot{\hat{V}}(\delta)d\delta = -\int_C \hat{F}\cdot dq = -\int_0^t \hat{F}\cdot\dot{q}d\delta \\ = & \int_0^t \hat{N}_3(\phi,\theta_a,\theta_k)\dot{\phi}d\delta + \int_0^t \hat{N}_4(\phi,\theta_a,\theta_k)\dot{\theta}_a d\delta \\ & + \int_0^t \hat{N}_5(\phi,\theta_a,\theta_k)\dot{\theta}_k d\delta \\ = & \int_{C_{0,t}} \hat{N}_3(\phi,\theta_a,\theta_k)d\phi + \int_{C_{0,t}} \hat{N}_4(\phi,\theta_a,\theta_k)d\theta_a \\ & + \int_{C_{0,t}} \hat{N}_5(\phi,\theta_a,\theta_k)d\theta_k,\end{aligned}$$

given the line integral in [37]. Since $\hat{V}$ is continuously differentiable, the conservative force vector $\hat{F}$ is also continuous. As a result, the integral $\int_0^t \hat{N}_3(\phi,\theta_a,\theta_k)\dot{\phi}d\delta$ is bounded in a finite time based on extreme value theorem.

In addition, according to [38], the work done by conservative force vector $\hat{F}(q)$ depends only on the endpoints but not the trajectory path of the state. For any state trajectories within range-of-motion during walking tasks, the integral $\int_0^t \hat{N}_3(\phi,\theta_a,\theta_k)\dot{\phi}d\delta = \int_{C_{0,t}} \hat{N}_3(\phi,\theta_a,\theta_k)d\phi = B_{0,t}$ depends only on the paths between the initial q_0 and final state q_t of $C_{0,t}$. Our assumption is reasonable for walking tasks, where for any time t and gait state trajectories C, we have $|\int_0^t \hat{N}_3(\phi,\theta_a,\theta_k)\dot{\phi}d\delta| = |\int_C \hat{N}_3 d\phi| \leq \max_C B_{0,t} = B_{\max}$ and the energy function $E(q,p) \geq 0$ for all states (q,p), where $B_{\max}$ is incorporated into E^0.

The time derivative of $E(q,p)$ is

$$\begin{aligned}\dot{E} = & (\nabla H^T + [\nabla_q \hat{V}^T, 0])\begin{bmatrix}\dot{q}\\ \dot{p}\end{bmatrix} - \hat{N}_3(\phi,\theta_a,\theta_k)\dot{\phi} \\ = & [\partial_q H^T + \nabla_q \hat{V}^T, \partial_p H^T])\begin{bmatrix}\partial_p H \\ -\partial_q H - \hat{N} + J_2 \partial_p H\end{bmatrix} \\ & + (\partial_p H)^T \tau_{\text{hum}} + (\partial_p H)^T A^T \tilde{\lambda} - \hat{N}_3(\phi,\theta_a,\theta_k)\dot{\phi} \\ = & \cancel{\nabla_q \hat{V}^T \partial_p H} - \cancel{\partial_p H^T \hat{N}} - \cancel{\hat{N}_3(\phi,\theta_a,\theta_k)\dot{\phi}} + (\partial_p H)^T \tau_{\text{hum}} \\ = & (\partial_p H)^T \tau_{\text{hum}},\end{aligned}$$

where we use the skew-symmetry property of the interconnection structure J_2 and $(\partial_p H)^T A^T \tilde{\lambda} = 0$ due to the fact that constraint forces do no work [39]. Thus, the system is passive from the human input τ_{hum} to the output $\partial_p H$. ■

Input-output passivity implies that the energy growth of the coupled human-exoskeleton system is controlled by the human. This provides safe interaction with the exoskeleton, but stability depends on the human control law. We utilize LaSalle's invariance principle (Theorem 4.4 from [27]) to prove the trajectory of the closed-loop system (3) approaches the invariant set as $t \to \infty$. We make the common assumption that the human is modulating joint impedance where $\tau_{\text{hum}} = -K_p e - K_d \dot{e}$ [17]. The constant diagonal matrices K_p, K_d are positive semi-definite, and $e = q - \bar{q}$ represents the difference between q and the human's set-point vector $\bar{q}$. We have the following proposition based on [27, Theorem 4.4]:

Proposition 2.2: Let $\mathscr{V}(q,p) = E + \frac{1}{2}e^T K_p e$, which is continuously differentiable and positive semi-definite (vanishes not only at the equilibrium point). Let $\Omega = \{[q^T, p^T]^T \in \mathbb{R}^{10} \mid \mathscr{V}(q,p) < c\}$, for any $c > 0 \in \mathbb{R}$. Let Γ be the largest invariant set in $\{[q^T, p^T]^T \in \mathbb{R}^{10} \mid \dot{\mathscr{V}}(q,p) = 0\} \subset \Omega$. Given human input $\tau_{\text{hum}} = -K_p e - K_d \dot{e}$, any trajectories of the system (3) starting in Ω approach Γ as $t \to \infty$.

Proof: The function $\mathscr{V}$ is radially unbounded, where $\frac{1}{2}p^T M^{-1} p + \frac{1}{2}e^T K_p e \to \infty$ as $\left\|[q^T, p^T]^T\right\| \to \infty$. As a result, the set Ω is bounded for all values of c according to [27]. We also have

$$\dot{\mathscr{V}} = (\partial_p H)^T \tau_{\text{hum}} + \dot{q}^T K_p e = -\dot{q}^T K_d \dot{q} \leq 0.$$

As a result, for (q,p) starting in Ω at $t = 0$, we have

$$\dot{\mathscr{V}} \leq 0 \Rightarrow \mathscr{V}(q(t),p(t)) \leq \mathscr{V}(q(0),p(0)) \leq c, \forall t \geq 0,$$

i.e., (q,p) remains in Ω. Thus, the set Ω is a compact, positively invariant set, which satisfies the sufficient conditions in [27, Theorem 4.4]. By using LaSalle's invariance principle, the proposition is proven. ■

The invariance guarantees the trajectories stay within an invariant set. However, it does not imply the stability of the system. Although ϕ is unactuated with respect to the muscles on the ipsilateral leg, the interaction forces with the rest of the body can actuate this DOF (especially during double support phase). If we assume that the human is modulating joint impedance [17] and compensating the missing gravitational component in $\hat{N}$, where

$$\tau_{\text{hum}} = -K_p e - K_d \dot{e} - [0, 0, \hat{N}_3(\phi,\theta_a,\theta_k), 0, 0]^T,$$

we can show the stability of the closed-loop system (3) around the equilibrium point $(q^\star, 0)$, where the forces along the shaped potential energy balance the muscular forces and the ground reaction forces. We can now state Proposition 2.3.

Proposition 2.3: Consider the closed-loop system (3), the equilibrium point $(q^\star, 0)$ is stable in the sense of Lyapunov given human input $\tau_{\text{hum}} = -K_p e - K_d \dot{e} - [0, 0, \hat{N}_3(\phi,\theta_a,\theta_k), 0, 0]^T$.

Proof: We can set the Lyapunov function $\mathscr{W}(q,p)$ to be

$$\mathscr{W} = H + \hat{V} + \frac{1}{2}e^T K_p e + \int_{q_0}^q A(s)^T \tilde{\lambda}(s,0)\cdot \mathrm{d}s - \mathscr{W}^0, \quad (11)$$

where q_0 is the state at $t = 0$ and $\mathscr{W}(q,p)^0$ is a constant such that $\mathscr{W}$ is positive definite and vanishes at the equilibrium point $(q^\star, 0)$. The Lyapunov function $\mathscr{W}$ achieves its minimal point when $\partial_p \mathscr{W} = \dot{q} = p = 0$ and $\partial_q \mathscr{W} = N + \nabla_q \hat{V} + K_p e + A^T \tilde{\lambda} = 0$, i.e., at the equilibrium point $(q^\star, 0)$. The incorporation of $\int_{q_0}^q A(s)^T \tilde{\lambda}(s,0)\cdot ds$ guarantees the appearance of the GRFs to balance the unactuated parts of $N + \nabla_q \hat{V}$ at the equilibrium state when $\partial_q \mathscr{W}(q,0) = 0$. As a result, the Lyapunov function $\mathscr{W}$ is positive definite and vanishes only at the equilibrium point $(q^\star, 0)$.

The time-derivative of Lyapunov function (11) is

$$\begin{aligned}\dot{\mathscr{W}} &= (\nabla H^T + [\nabla_q \hat{V}^T, 0]) \begin{bmatrix}\dot{q}\\ \dot{p}\end{bmatrix} + \dot{q}^T K_p e + \dot{q}^T A^T \tilde{\lambda}(q,0) \\ &= \nabla_q \hat{V}^T \partial_p H - \partial_p H^T \hat{N} + (\partial_p H)^T \tau_{\text{hum}} + \dot{q}^T K_p e \\ &= \cancel{\nabla_q \hat{V}^T \partial_p H} - \cancel{\partial_p H^T \hat{N}} + (\partial_p H)^T (-K_p e - K_d \dot{e} \\ &\quad \cancel{- [0,0,\hat{N}_3(\phi,\theta_a,\theta_k),0,0]^T}) + \dot{q}^T K_p e \\ &= -\dot{q}^T K_d \dot{q} \leq 0,\end{aligned}$$

which shows that the shaped system is Lyapunov stable. ■

As mentioned in [28], Lyapunov stability ensures the response will remain in a neighborhood of the equilibrium under human impedance control with compensation of balancing moment. This result satisfies our control objective of partial torque assistance while the human controls their kinematics.

III. Results

We now show optimization results to demonstrate the proposed controller's ability to recreate normative torques for different tasks, including walking on level-ground, ramps, stairs, and sit-stand cycle. We also experimentally implement the controller on a knee-ankle exoskeleton used by multiple healthy human subjects.

A. Design Optimization

We propose two shaping strategies: 1) Hamiltonian without ϕ (WOP) has basis functions depending on θ_a and θ_k only, and 2) Hamiltonian with ϕ (PHI) has the global variable ϕ incorporated into the basis functions. The basis functions ξ associated with WOP comprise combinations of sine and cosine functions of θ_a and θ_k and satisfy Proposition 2.1 in [28]. PHI has ϕ incorporated with 67 basis functions, where the list of basis functions for the ankle and the knee joints $\xi_{\text{ankle}}, \xi_{\text{knee}} \in \mathbb{R}^{67\times 1}$ are shown as follows

$$\begin{aligned}\xi_{\text{ankle}} = [&1, 0, \sin(\theta_a), \cos(\theta_a), 0, 0, \sin(\theta_a+\theta_k), \ldots, \\ &\sin(\phi+\theta_a+2\theta_k)\dot{\theta}_k, \cos(\phi+\theta_a+2\theta_k)\dot{\theta}_k] \\ \xi_{\text{knee}} = [&0, 1, 0, 0, \sin(\theta_k), \cos(\theta_k), \sin(\theta_a+\theta_k), \ldots, \\ &-\sin(\phi+\theta_a+2\theta_k)\dot{\theta}_a, -\cos(\phi+\theta_a+2\theta_k)\dot{\theta}_a],\end{aligned}$$

The WOP method has all the terms related to ϕ removed, where the total number of the basis functions equals 35. We have $\Phi(q,p) = [\xi_{\text{ankle}}^T, \xi_{\text{knee}}^T]^T \in \mathbb{R}^{2\times w}$ in (8). Column vectors in $\Phi(q,p)$ associated with the shaped gyroscopic terms are orthogonal to $[\dot{\theta}_a, \dot{\theta}_k]^T$. In contrast, column vectors in $\Phi(q,p)$ associated with the shaped potential energy introduce a combination of modified gravitational potential energy and nonlinear springs that provides conservative force vector following the normative torques. The weighting matrix in (9) adjusts how we want the controller to provide the desired assistant torques. We optimize the constant coefficients α to fit the control law outputs to the across-subject averaged human joint moments over level-ground, ramps, stairs walking, and stand-to-sit [40], [41]. vGRFs from [40] are normalized by the body weight, whereas [41] does not provide vGRFs, and we set it to be a constant value during the optimization process. The training tasks include level walking on treadmill with $0.5, 1.5\text{m/s}$, ramp ascent/descent walking with $5.2^\circ, 11^\circ$, stairs ascent/descent walking with $4, 7$inch step height [40], and the stand-to-sit task in [41]. The testing (validation) tasks include level walking on treadmill with 0.65m/s, ramp ascent/descent walking with 9.2°, stairs ascent/descent walking with 6inch step height, transition between stairs ascent/descent walking to level walking with 6inch step height [40]. For the normative torque associated with the knee during stand-to-sit, we keep it at maximum during the late sit phase for real-time implementation. The controller can provide adequate assistance, and the user can adjust the assistance based on vGRFs. The process provides the optimal parameters α^*, where we neglect those parameters with absolute values contributing less than $0.1\% \cdot \|\alpha^*\|_2$ (depending on the number of parameters neglected). Fig. 3 shows the agreement between a single energy-shaping control strategy (exoskeleton torque τ_{exo}) and normative human torques τ_{hum} over multiple activities of daily living.

B. Comparison to Ideal Finite State Machine

The performance of the proposed method is evaluated by comparing an ideal finite-state machine (FSM) for testing tasks. We define FSM in a similar way as in [42], where the ideal FSM is assumed to provide the normative human torque with pre-defined tasks using intent recognition between different modes, including walking and stairs climbing. The pre-defined tasks include level walking on treadmill with 1.5m/s, ramp ascent/descent walking with 5.2°, stairs ascent/descent walking with 4inch step height in [40] to cover the majority training tasks. For testing tasks, the ideal FSM returns a torque profile in the database (pre-defined tasks) that achieves minimum cost and most closely matches the normative human torque. The problem is defined as finding $j \in \{1,\ldots,M\}$ in the pre-defined tasks motivated by [42, Equation (7)]

$$\arg\min_j \left\| Y_i - Y_j \right\|_2, \ \forall i \in \{1,\ldots,L\},$$

which yields for testing task Y_i. This FSM is hard to achieve in real time, however, it provides a useful standard of comparison representing the minimum possible error with the FSM approach [42], [43].

We use two metrics for comparison of the proposed and FSM methods. The first metric used is a cosine similarity which is a judgment of orientation that measures the pattern of the normative torques. The second metric used is the VAF which measures the variability of the data that can be explained by a fitted regression model. The definition is given as follows

$$\begin{aligned}\text{similarity}(A,B) &= 100 \cdot \frac{A \cdot B}{\|A\|_2 \|B\|_2} \\ \text{VAF}(A,B) &= 100 \cdot \left(1 - \frac{\|A-B\|_2^2}{\|A\|_2^2}\right)\end{aligned}$$

As shown in Table I, both the PHI and WOP methods perform well with different walking tasks under the metric of the similarity and VAF, with minor improvements of the PHI

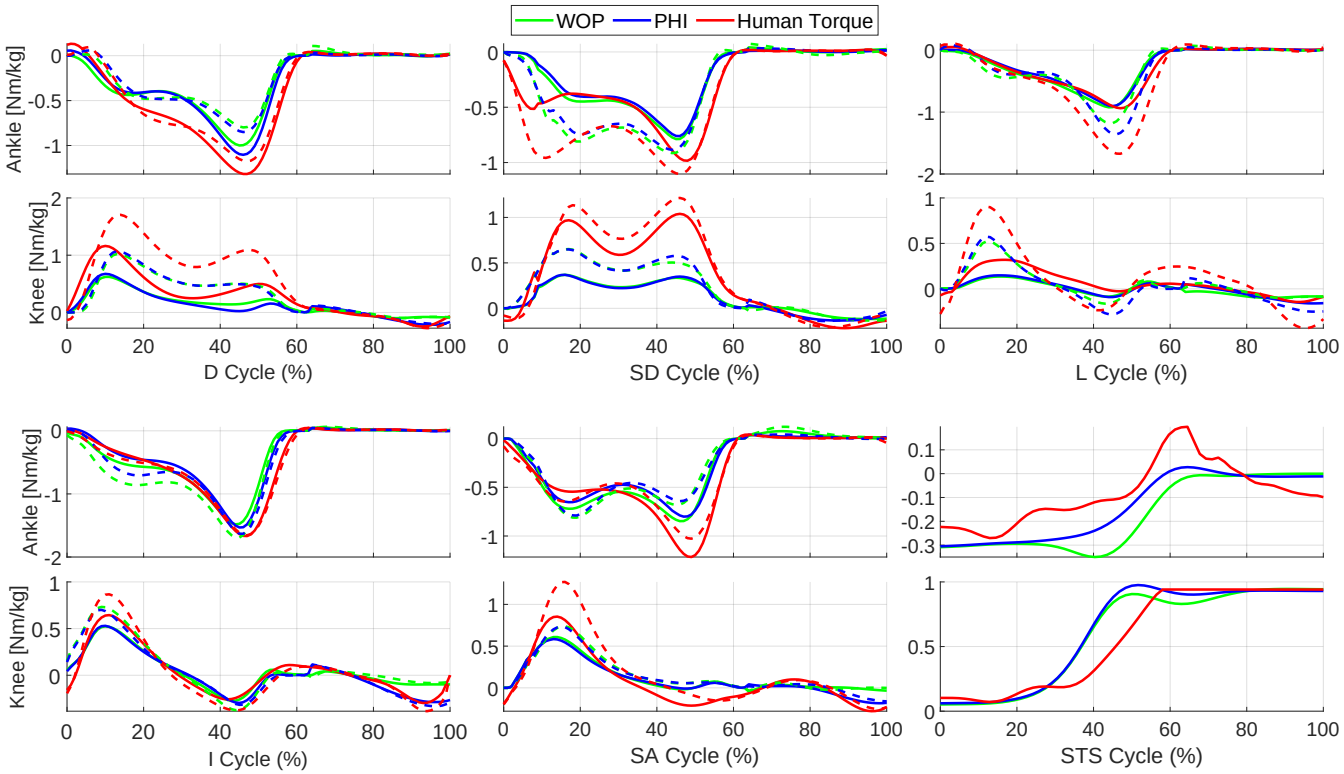

Fig. 3. Exoskeleton control torques and normative human torques based on human treadmill walking (L) 0.5m/s (solid lines), 1.5m/s (dash lines), ramp ascent/descent (I/D) 5.2° (solid lines), 11° (dash lines), stairs ascent/descent (SA/SD) 4inch (solid lines), 7inch (dash lines), and stand-to-sit (STS). Positive values represent ankle dorsiflexion and knee extension.

TABLE I

COMPARISON OF TECHNIQUES. L, I/D, SA/SD, SD-W/SA-W, AND STS REPRESENT LEVEL-GROUND WALKING, RAMP ASCENT/DESCENT WALKING, STAIR ASCENT/DESCENT WALKING, STAIR DESCENT/ASCENT WALKING TO LEVEL WALKING TRANSITIONS, AND STAND-TO-SIT. POSITIVE AND NEGATIVE VALUES REPRESENTING ASCENT AND DESCENT, RESPECTIVELY.

Training Data

Tasks	Similarity(%)		VAF(%)	
	WOP	PHI	WOP	PHI
L 0.5m/s	95.33	96.97	90.86	93.52
L 1.5m/s	94.40	97.34	79.92	88.18
D −5.2°	97.03	96.45	82.96	84.73
D −11°	98.45	98.47	80.66	82.37
I 5.2°	95.67	98.10	90.87	94.88
I 11°	93.65	97.07	86.76	94.18
SD −4in	88.95	90.02	69.07	68.56
SD −7in	93.28	94.54	80.43	80.96
SA 4in	93.60	95.64	86.22	87.60
SA 7in	91.75	93.62	81.76	83.43
STS	96.44	97.39	91.98	93.61

Testing Data

Tasks	Similarity(%)			VAF(%)		
	WOP	PHI	FSM	WOP	PHI	FSM
L 0.65m/s	94.38	96.37	88.70	88.26	91.39	68.39
R −9.2°	98.30	98.28	94.37	82.24	83.64	87.80
R 9.2°	94.49	97.65	98.66	89.14	95.03	97.14
SD −6in	92.22	93.38	93.89	80.58	80.88	87.22
SA 6in	92.62	93.81	90.06	83.45	83.77	81.10
SD-W −6in	88.88	90.12	89.88	78.95	80.84	79.21
SA-W 6in	88.67	91.00	95.41	78.62	82.55	90.31
Mean	92.79	94.37	93.00	83.03	85.44	84.45

method. On the other hand, the FSM method outperforms the proposed methods over ramp ascent walking with 9.2°. The reason is due to the minor change of joint torques in ramp ascent walking between different incline angles, i.e., the testing data of 9.2° matches close to the pre-defined tasks. However, for the testing tasks not matching close to any pre-defined tasks, the performance drops dramatically, for instance, ramp descent walking with −9.2° and the transition from stair-descent to level-ground walking. The performance of our proposed methods can be further improved by training with all data (including the testing data), while the FSM, on the other hand, is always limited to one condition per activity. For experimental implementation, we use the training data (multiple conditions per activity) in Section III-A and withhold the other data in [40] to help avoid overfitting in addition to the L1 regularization.

C. Experimental Test with Healthy Human Subjects

1) Implementation: The controller was implemented on a 4.5 kg partial-assist knee-ankle exoskeleton (*Comex* [17], [44], Fig. 1) to evaluate the performance for providing appropriate assistance over multiple activities of daily living. Mass specifications of the powered knee-ankle exoskeleton are summarized in [17, TABLE 1], where the knee module (thigh) weighs 2.106 kg, and the ankle module (shank) weighs 1.843 kg, including the mass of onboard electronics and cabling. The actuators are backdrivable due to a low 24:1 gear ratio and produce 30 Nm continuous torque

(60 Nm peak) using a 200 W frameless BLDC motor. The transmission comprises a belt stage and a custom planetary gearbox inside the driven sprocket. The motors are driven with sinusoidal commutation by Elmo Gold Twitter drives (rated to 30 A). The control system includes the onboard sensors and computation needed to implement torque control laws, including Sunrise torque sensors for closed-loop torque control running at 800 Hz on a National Instruments myRIO microcontroller. High-resolution magnetic incremental encoders (6400 CPR, LM13, Renishaw, Inc.) measure joint angles/velocities, and a 6-axis Microstrain inertial measurement unit (IMU, Lord Microstrain) measures orientation. An onboard Lithium-Ion battery pack powers the system. The device also includes safety features such as hard stops and current limiters at both joints.

The unpowered backdrive torque is about 3 Nm, allowing the user to control their joint kinematics freely. The active modes in [28] did not reduce muscle activation of tibialis anterior, where the assistive dorsiflexion torques in the swing phase ($>60\%$ stride) were lower than the estimated backdrive torque (3 Nm, see [17, Fig. 16]), suggesting the subject experienced more resistance than assistance. The peak dynamic backdrive torque can reach 5 Nm at the ankle during uncompensated fast walking. We utilize the methods mentioned in [45] to reduce the backdriving torque acting on the ankle joint for a broad range of accelerations and velocities, covering the requirements for rehabilitation applications without the additional use of expensive force-torque sensors. The inertia compensation depends on the acceleration together with the moment of inertia of the motor. The torques induced by inertia are calculated through

$$\tau_{\text{inertia, ankle}} = \ddot{\theta}_a \cdot I_{\text{reflected inertia}}.$$

The reflected inertia is approximated by the rotor inertia times the gear ratio squared [46]. For *Comex*, the reflected inertia $I_{\text{reflected inertia}}$ equals 691.5kg-cm^2. We apply the inertia compensation when $\ddot{\theta}_a \geq 0$ to assist tibialis anterior during dorsiflexion and avoid oscillation of the control inputs around $\ddot{\theta}_a = 0$. We saturate the inertia compensation within $\tau_{\text{inertia, ankle}[0,2.5]} \in [0, 2.5]$ for the ankle to prevent excessive inertia compensation. Since the control law provides small dorsiflexion torques during the gait cycle as shown in Fig. 3, we also amplify the optimal control input $u_{\text{optimal, ankle}}$ when the assistive dorsiflexion torques are lower than the estimated backdrive torque (3 Nm). This can compensate for the backdrive torque acting on the ankle joint. For dorsiflexion torques higher than the estimated backdrive torque, the optimal control input $u_{\text{optimal, ankle}}$ remains unchanged. The commanded control input of the ankle and knee joints is summarized as if $u_{\text{optimal, ankle}} \in [0, 3]$,

$$\begin{aligned} u_{\text{ankle}} &= 1.3 \cdot u_{\text{optimal, ankle}} + \tau_{\text{inertia, ankle}[0,2.5]}, \\ u_{\text{knee}} &= u_{\text{optimal, knee}}, \end{aligned}$$

otherwise

$$\begin{aligned} u_{\text{ankle}} &= u_{\text{optimal, ankle}} + \tau_{\text{inertia, ankle}[0,2.5]} \\ u_{\text{knee}} &= u_{\text{optimal, knee}}, \end{aligned}$$

where $u_{\text{optimal, ankle}}, u_{\text{optimal, knee}}$ comes from (8), and are determined by multiplying the optimized control law (in Nm/kg) with the subject's body weight and a LOA%. The scaling value 1.3 and saturation number 2.5 are based on the subjects' comfort level during the practice trials.

vGRF feedback to the optimized control law is measured by a custom force sensor in the *Comex* footplate as in [31]. The foot sensor was designed to record the wearer's vertical ground reaction force with the accuracy of a force plate while maintaining the profile and level of portability necessary to incorporate into the underfoot region of *Comex*'s footplate [31, Fig. 2]. This was accomplished using a structure inspired by force plate construction, wherein each section includes two rigid plates, held apart by circular spacers (pucks) that each sits atop a FlexiForce A401 (Tekscan, South Boston, MA) force-sensitive resistor (FSR). Due to the gap between the rigid plates being held open by the pucks, all force applied to the plates' large surface areas travels through the pucks and, as a result, the FSRs. A thin layer of compressible foam is placed above and below the FSRs to ensure sufficient pressure distribution between the puck and the lower plate. The FSRs from the heel and middle section of the sensor are connected in parallel and form the total heel resistance. Similarly, the three FSRs from the toe section are connected in parallel, forming the total toe resistance. The change in resistance of the heel and toe (related to the force being applied at these locations) is sensed and amplified by an operational amplifier circuit recommended in the Tekscan data sheet [47]. This circuit also linearizes the nonlinear resistance-force relationship. Finally, MyRIO software is used to calibrate the sensors before each experiment to achieve a final readout normalized to body weight, where vGRFs from dataset are also normalized in the same way. The final values of vGRFs are saturated within $[0, 1]$ in MyRIO LabVIEW code [48] to avoid excessive assistant torques for safety concern. Before starting recording the data for real-time experiments, we tested the controller with several practice trials and adjusted the optimization process with different weighting factors in (9) for the subject's comfort. The iteration between the trials and the tests returned the ultimate optimal parameters for the controller that provides proper torque assistance on multiple tasks.

2) Methods: We enrolled five human subjects (s1, male, mass: 78 kg, height: 1.78 m;s2, male, mass:75 kg, height: 1.75 m;s3, female, mass: 50 kg, height: 1.62 m;s4, male, mass: 83 kg, height: 1.79 m;s5, female, mass: 60 kg, height: 1.75 m) to demonstrate the controller's ability to assist musculature for multiple tasks. Two subjects (s4, s5) were excluded due to the failure of a foot FSR causing unusual command torques, which was only noticed after the experiment. The study was approved by the Institutional Review Board at the University of Michigan (HUM00164931). We assessed muscle activation via electromyography (EMG) of vastus medialis oblique (VMO), rectus femoris (RF), biceps femoris (BF), tibialis anterior (TA), gastrocnemius (GM), and soleus (SOL), which respectively function as a knee extensor, knee extensor/hip flexor, knee flexor, dorsiflexor, plantarflexor/knee flexor, and plantarflexor respectively.

The experiment consisted of five treadmill walking tasks at subject preferred speeds, sit-to-stand/stand-to-sit tasks, and two indoor stairs walking tasks as follows: level walking at speed of 1 m/s (subject 3 chose 0.8 m/s), incline/decline walking on a $\pm 5.2^{\circ}$ slope at 0.6 m/s, incline/decline walking on a $\pm 12.4^{\circ}$ slope at 0.6 m/s, a repetitive sit-stand cycle using a metronome set to 45 beats-per-minute (BPM), and stairs ascent/descent walking on 7 inch step height with metronome (60 BPM). The tasks were repeated for three exoskeleton modes: bare (no exoskeleton), active exoskeleton with ϕ incorporated (PHI), and active exoskeleton without ϕ incorporated (WOP). At least 30 gait cycles were collected for each mode for the treadmill tasks, 18 gait cycles for the stairs tasks, and a total of 18 repetitions were carried out for the sit-stand-sit trials. Use of the treadmill handrails was disallowed during the experimental trials. The LOA% for the active modes was set to 60% for subject 1 (s1) and 50% for other subjects, based on the subjects' comfort level during the practice trials.

The walking trials were cropped into gait cycles by utilizing a heel-mounted accelerometer to determine heelstrike. Sit-stand-sit trials were cropped into individual repetitions by utilizing a thigh-mounted accelerometer built into the EMG sensor. For each task, each muscle's EMG was demeaned, bandpass filtered (20 - 200 Hz), rectified, smoothed with a moving 100 ms window RMS, and then normalized with respect to the maximum peak of the ensemble averages (across repetitions) of the three modes [49]. This was done for each task and muscle separately, resulting in the signals being converted to a percentage of the maximum voluntary contraction level (%MVC) for a consistent and fair comparison across different subjects. After normalizing the EMG to % MVC, the integral with respect to time was calculated to represent muscular effort as % MVC.s, similar to [31].

3) Results: Our subjects had vast (s1), moderate (s2), or minimal (s3) experience with *Comex*. The ensemble-averaged VMO, RF, BF, TA, GM, and SOL EMGs for bare and active modes are shown in Fig. 4 for s1, and Fig. 5 for across-subjects averaged comparison. In general, the dominant muscles in the stance phase (VMO, GM, and SOL) had reduced effort for the active modes, compared to the bare mode for most tasks. Moreover, the assistance torque profiles matched the muscle activation profiles, explaining the reduction in muscle activation compared to bare mode.

Incline walking and stairs ascent is primarily associated with positive power or concentric muscle contractions. In these tasks, the quadriceps are predominantly activated to lift the center of mass (COM) of the body. Both PHI and WOP provided knee extension torques in this phase and resulted in a noticeable EMG reduction of the VMO for s1 and s2. Both controllers provided plantar-flexion torques in this phase for stairs ascent and incline walking, resulting in a noticeable GM as well as SOL EMG reduction compared to the bare mode for s1 and s2 with stairs ascent. For s3, there is only a noticeable reduction in this phase for SOL with incline walking. These results may improve with adaptation.

Stairs descent and decline walking are primarily associated with negative power and involve eccentric quadriceps and plantar-flexor contractions. Commonly, a double peak quadriceps activation profile is apparent in stance; firstly to absorb the impact of heel strike, and secondly to lower the COM. Both controllers provided knee extension torques during these phases, which resulted in substantial EMG reductions compared to the bare mode of the VMO for s1 with all stairs descent and decline walking tasks, and s2 and s3 with most stairs descent and decline walking tasks. Both controllers provided substantial plantar-flexion assistance torques during mid to late stance to assist with the negative work of lowering the COM. This resulted in substantial reductions in SOL activity compared to the bare mode for s1 with all stairs descent and decline walking tasks, and s2 with most stairs descent and decline walking tasks. Note that the SOL is more active during flexed knee positions (such as decline walking or stairs descent) than GM, which is more active during extended knee positions.

Sit-to-stand and stand-to-sit primarily require knee extension torques [50]. During sit-to-stand, these occur in the form of concentric contractions, and during stand-to-sit, as eccentric contractions. Both controllers provided substantial knee extension torques, resulting in a noticeable reduction in VMO (knee extensor) activations for s1 and s2. Results of GM and SOL have inter-subject variability due to the low muscle activation in the sit-stand cycle compared to the dominant muscles (VMO and RF).

Lastly, we observed muscle activation reductions during level walking both in the quadriceps and the plantar-flexors during stance. The quadriceps have a high activation in bare mode primarily to dampen the impact of heel strike. The plantar-flexors provide the pushoff power during late stance to drive the COM forwards. Both our controllers provided appropriate knee extension and plantar-flexion assistance torques that resulted in noticeable reductions in VMO (s1) and SOL (s2) activity in the stance phase. Since the knee goes through a minimal range of motion during stance in level walking, our prior controller that utilized only potential energy shaping was not adequate to provide assistance during this phase. With the PHI and WOP controllers developed in the present study, adequate knee extension assistance torques are provided to assist with impact absorption in early stance.

The TA activations for both PHI and WOP are higher than bare throughout the stride cycles for all walking tasks. This is similar to the results in [51], where the TA during the swing phase had increased activity with decreasing gravity. One explanation is that we are not providing adequate torques to support the weight of the sensorized exoskeleton foot plate. It is also possible that the provided plantar-flexion torques are excessive, necessitating the TA activation to compensate. Future work will model the passive dynamics of the muscle-tendon unit (MTU) for all joints. This is especially important for the ankle, i.e., the Achilles tendon is known to provide significant storage and release of energy, much like a spring.

BF's purpose during the swing is to lift the foot by flexing the knee and aids in leg clearance. Although we provided marginal knee flexion torques, we observed very high activations for the BF with the active modes compared to bare, which is also found in [51] for BF in the stance

phase. A potential explanation can be the interaction with its second function as a hip extensor and needing to carry the added weight of the exoskeleton during the swing, which can also affect RF performance.

The observations in Fig. 5 and Fig. 6 meet our simulation expectations and demonstrate the potential to assist musculature in multiple tasks. Note that the EMG signal is normalized with respect to the maximum peak of the ensemble averages as %MVC, which does not reflect the difference of muscle activations between dominant and non-dominant muscles for each task. For instance, during decline walking (-12.4°), VMO is dominant and has a large reduction in EMG with active modes, whereas the non-dominant BF has the opposite effect. We believe that improvement in dominant muscles carries more weight than worsening of non-dominant muscles when assessing the overall performance of the proposed methods. Fig. 7 shows that the averaged command torques (PHI and WOP methods) match with the normative human torques from [40], [41] in most tasks, where we apply L2 normalization to the torque dataset values for a better comparison with respect to different LOA%. The mismatch in some tasks may be caused by the mismatch of feedback joint angles and IMU information. In addition, the vGRFs were measured by the custom force sensor in the *Comex* footplate and saturated between $[0,1]$, which feedback different values from the one used in the simulation. Fig. 8 shows subject-wise muscular efforts, demonstrating that s1 and s2 responded better to orthosis assistance than s3 for some muscles and tasks. Prior studies that showed EMG reductions gave the user adequate time to adapt under the assistance [52], which suggests the human subjects' outcomes may improve by providing more acclimation time. In addition, the effect of the subject's height and weight may correlate with the results, where the knee and ankle modules of the exoskeletons should be well-aligned and tightly attached to the thigh and shank, respectively. Additional human subjects would be needed to draw more general conclusions about the controller's effectiveness, which is left to future work.

IV. Conclusion

This paper applied the novel energetic control strategy based on the IDA-PBC method for a backdrivable knee-ankle exoskeleton with multiple tasks, including level-ground, ramps, stairs walking, and sit-stand cycle. In [28], the modified gravitational vector $\hat{N}$ depends only on the actuated variables θ_a and θ_k. The corresponding potential energy shaping controller behaves as nonlinear springs, which does not consider the global variable of the human-exoskeleton system, i.e., the gravity's direction. We incorporated the global variable into the controller with proof of the input-output passivity and stability of the closed-loop system. We increased the candidate basis functions in the optimization process, which achieves an optimal controller that fits normative human joint torques more closely. We considered "L1 regularization", which fits the data with as few parameters as possible to avoid overfitting problems. Our model assumes the stance leg is fully loaded with the user's weight. This results in excessive plantar-flexion torques as weight transfers from the assisted leg to the contralateral leg during double support. We solved this issue by considering vGRFs in the basis functions for optimization. The optimal controller was assessed in terms of the similarity and VAF to normative human torques in the simulation. We assessed the muscular effort of multiple able-bodied human subjects with the first experimental implementation of TES on an exoskeleton with consideration of level-ground, ramps, stairs walking, and sit-stand cycle.

The feedback of joint angles and IMU into the controller resulted in some variance with respect to the normative torques in the simulation. Future work should consider the consistency between the data in the simulation and data acquired from the real-time experiment. Moreover, matching the normative human torques reduced several muscle activations, while other muscle units had increased activations probably due to the co-contraction or compensation of the exoskeleton's weight. Future work should also account for the force components provided by the muscle-tendon unit instead of only using joint moments.

Acknowledgment

The authors thank Erica Santos for her assistance.

References

[1] G. Zeilig, H. Weingarden, M. Zwecker, I. Dudkiewicz, A. Bloch, and A. Esquenazi, "Safety and tolerance of the rewalk™ exoskeleton suit for ambulation by people with complete spinal cord injury: a pilot study," *The journal of spinal cord medicine*, vol. 35, no. 2, pp. 96–101, 2012.

[2] S. A. Kolakowsky-Hayner, J. Crew, S. Moran, and A. Shah, "Safety and feasibility of using the eksotm bionic exoskeleton to aid ambulation after spinal cord injury," *J Spine*, vol. 4, p. 003, 2013.

[3] M. Hassan, H. Kadone, T. Ueno, Y. Hada, Y. Sankai, and K. Suzuki, "Feasibility of synergy-based exoskeleton robot control in hemiplegia," *IEEE Transactions on Neural Systems and Rehabilitation Engineering*, vol. 26, no. 6, pp. 1233–1242, 2018.

[4] O. Harib, A. Hereid, A. Agrawal, T. Gurriet, S. Finet, G. Boeris, A. Duburcq, M. E. Mungai, M. Masselin, A. D. Ames *et al.*, "Feedback control of an exoskeleton for paraplegics: Toward robustly stable, hands-free dynamic walking," *IEEE Control Systems Magazine*, vol. 38, no. 6, pp. 61–87, 2018.

[5] T. Yan, M. Cempini, C. M. Oddo, and N. Vitiello, "Review of assistive strategies in powered lower-limb orthoses and exoskeletons," *Robotics and Autonomous Systems*, vol. 64, pp. 120–136, 2015.

[6] N. C. Bejarano, S. Maggioni, L. De Rijcke, C. A. Cifuentes, and D. J. Reinkensmeyer, "Robot-assisted rehabilitation therapy: recovery mechanisms and their implications for machine design," *Emerging Therapies in Neurorehabilitation II*, pp. 197–223, 2016.

[7] R. Jimenez-Fabian and O. Verlinden, "Review of control algorithms for robotic ankle systems in lower-limb orthoses, prostheses, and exoskeletons," *Medical engineering & physics*, vol. 34, no. 4, pp. 397–408, 2012.

[8] D. Quintero, D. J. Villarreal, D. J. Lambert, S. Kapp, and R. D. Gregg, "Continuous-phase control of a powered knee–ankle prosthesis: Amputee experiments across speeds and inclines," *IEEE Transactions on Robotics*, vol. 34, no. 3, pp. 686–701, 2018.

[9] A. Duschau-Wicke, T. Brunsch, L. Lunenburger, and R. Riener, "Adaptive support for patient-cooperative gait rehabilitation with the lokomat," in *2008 IEEE/RSJ International Conference on Intelligent Robots and Systems*. IEEE, 2008, pp. 2357–2361.

[10] H. Zhu, C. Nesler, N. Divekar, V. Peddinti, and R. Gregg, "Design principles for compact, backdrivable actuation in partial-assist powered knee orthoses," *IEEE/ASME Transactions on Mechatronics*, 2021.

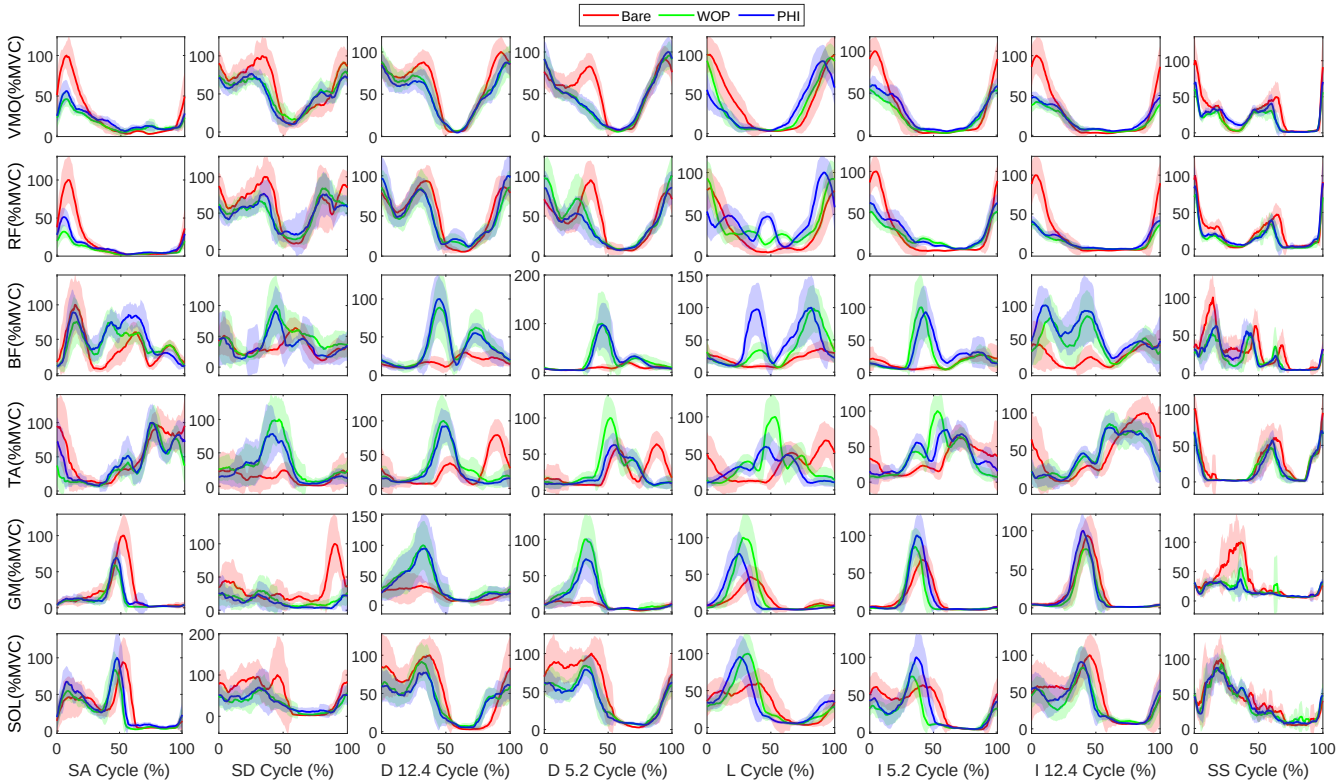

Fig. 4. Subject 1 EMG comparisons between bare and active modes (PHI and WOP methods) for each muscle (VMO, RF, BF, TA, GM and SOL) and task {decline $(-5.2^\circ, -12.4^\circ)$ and incline $(5.2^\circ, 12.4^\circ)$ at 0.6 m/s, level ground (1 m/s), Stairs Ascent/Descent (7in step height), and Sit-Stand cycle}. The red solid (bare), blue solid (PHI method), and green solid (WOP method) lines represent the time-normalized ensemble averages across all repetitions.

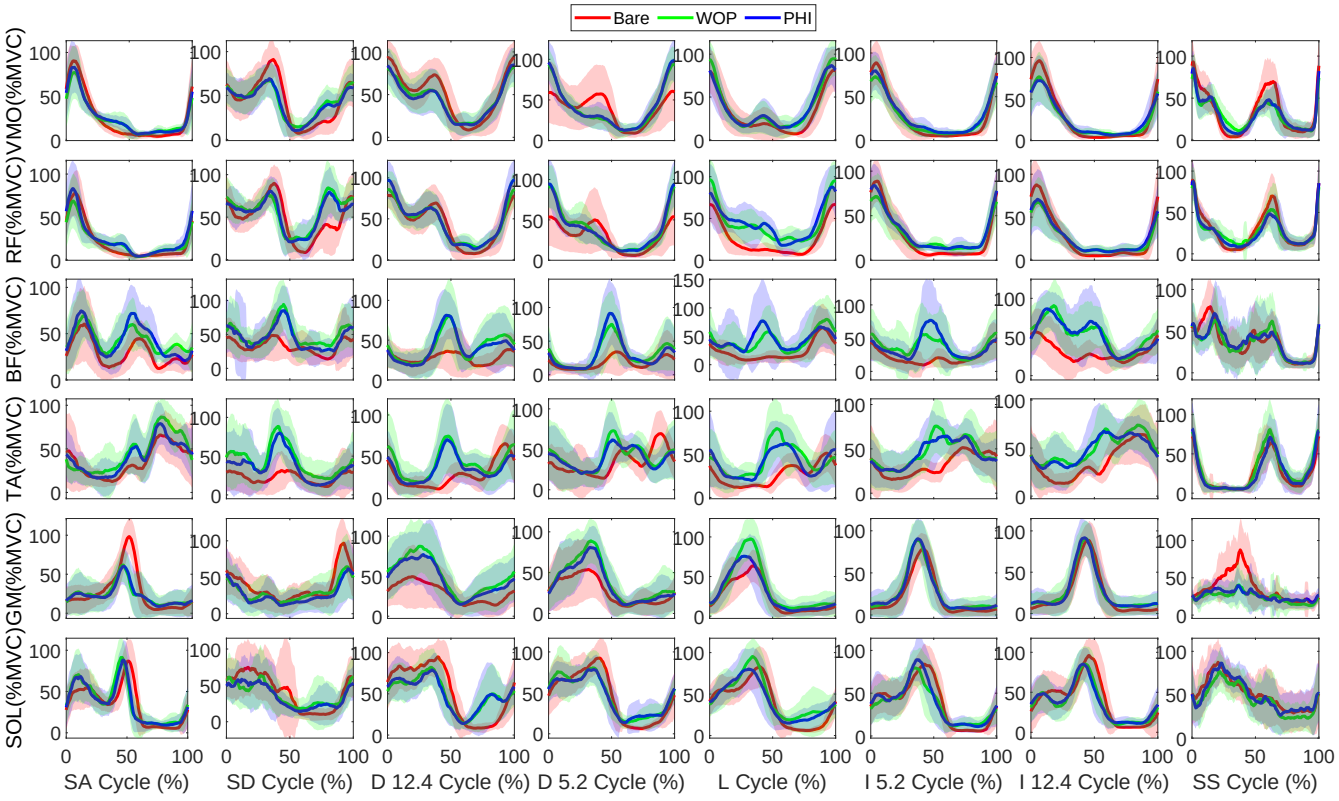

Fig. 5. Across-subjects averaged EMG comparisons between bare and active modes (PHI and WOP methods) for each muscle (VMO, RF, BF, TA, GM and SOL) and task {decline $(-5.2^\circ, -12.4^\circ)$ and incline $(5.2^\circ, 12.4^\circ)$ at 0.6 m/s, level ground (combined 0.8 m/s and 1 m/s), Stairs Ascent/Descent (7in step height), and Sit-Stand cycle}. The red solid (bare), blue solid (PHI method), and green solid (WOP method) lines represent the time-normalized ensemble averages across all repetitions.

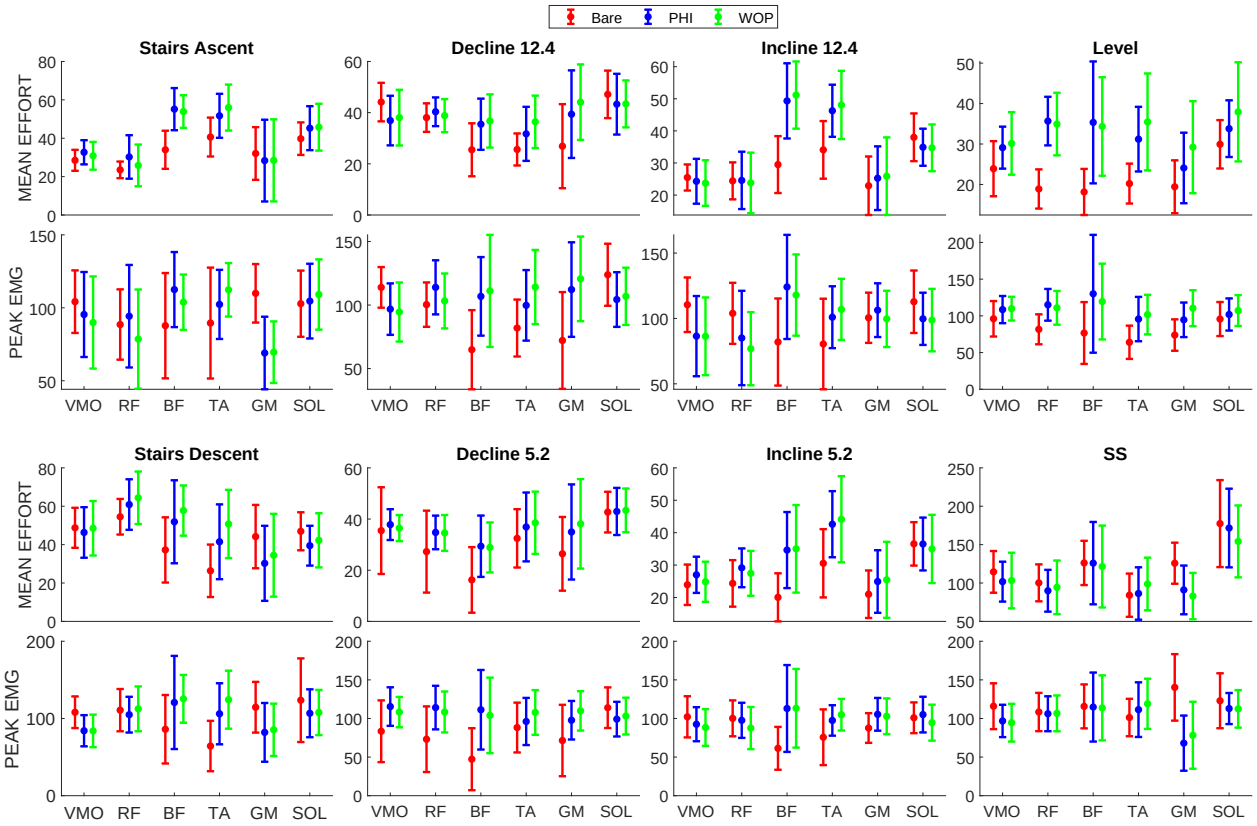

Fig. 6. Across-subjects mean effort (%MVC.S) and peak EMG (%MVC) comparisons for VMO, RF, BF, TA, GM and SOL: showing mean (± SD) for different tasks and muscles (columns).

[11] S. Chen, Z. Chen, B. Yao, X. Zhu, S. Zhu, Q. Wang, and Y. Song, "Adaptive robust cascade force control of 1-dof hydraulic exoskeleton for human performance augmentation," *IEEE/ASME Transactions on Mechatronics*, vol. 22, no. 2, pp. 589–600, 2016.

[12] B. He, G. C. Thomas, N. Paine, and L. Sentis, "Modeling and loop shaping of single-joint amplification exoskeleton with contact sensing and series elastic actuation," in *2019 American Control Conference (ACC)*. IEEE, 2019, pp. 4580–4587.

[13] U. Nagarajan, G. Aguirre-Ollinger, and A. Goswami, "Integral admittance shaping: A unified framework for active exoskeleton control," *Robotics and Autonomous Systems*, vol. 75, pp. 310–324, 2016.

[14] G. Aguirre-Ollinger, J. E. Colgate, M. A. Peshkin, and A. Goswami, "Inertia compensation control of a one-degree-of-freedom exoskeleton for lower-limb assistance: Initial experiments," *IEEE Transactions on Neural Systems and Rehabilitation Engineering*, vol. 20, no. 1, pp. 68–77, 2012.

[15] S. A. Murray, K. H. Ha, C. Hartigan, and M. Goldfarb, "An assistive control approach for a lower-limb exoskeleton to facilitate recovery of walking following stroke," *IEEE Transactions on Neural Systems and Rehabilitation Engineering*, vol. 23, no. 3, pp. 441–449, 2014.

[16] S. Yu, T.-H. Huang, X. Yang, C. Jiao, J. Yang, Y. Chen, J. Yi, and H. Su, "Quasi-direct drive actuation for a lightweight hip exoskeleton with high backdrivability and high bandwidth," *IEEE/ASME Transactions on Mechatronics*, vol. 25, no. 4, pp. 1794–1802, 2020.

[17] G. Lv, H. Zhu, and R. D. Gregg, "On the design and control of highly backdrivable lower-limb exoskeletons: A discussion of past and ongoing work," *IEEE Control Systems Magazine*, vol. 38, no. 6, pp. 88–113, 2018.

[18] A. M. Bloch, N. E. Leonard, and J. E. Marsden, "Stabilization of mechanical systems using controlled lagrangians," in *Decision and Control, 1997., Proceedings of the 36th IEEE Conference on*, vol. 3. IEEE, 1997, pp. 2356–2361.

[19] R. Ortega, A. Loría, P. J. Nicklasson, and H. J. Sira-Ramirez, *Passivity-based control of Euler-Lagrange systems*. Springer-Verlag, 1998.

[20] G. Lv and R. D. Gregg, "Towards total energy shaping control of lower-limb exoskeletons," in *American Control Conference (ACC), 2017*. IEEE, 2017, pp. 4851–4857.

[21] ——, "Underactuated potential energy shaping with contact constraints: Application to a powered knee-ankle orthosis," *IEEE Transactions on Control Systems Technology*, vol. 26, no. 1, pp. 181–193, 2018.

[22] J. Lin, G. Lv, and R. D. Gregg, "Contact-invariant total energy shaping control for powered exoskeletons," in *American Control Conf.* IEEE, 2019, pp. 664–670.

[23] G. Lv, H. Xing, J. Lin, R. D. Gregg, and C. G. Atkeson, "A task-invariant learning framework of lower-limb exoskeletons for assisting human locomotion," in *2020 American Control Conference (ACC)*. IEEE, 2020, pp. 569–576.

[24] G. Lv, J. Lin, and R. D. Gregg, "Trajectory-free control of lower-limb exoskeletons through underactuated total energy shaping," *IEEE access*, 2021.

[25] Wikipedia, "http://en.wikipedia.org/wiki/Computational$_{c}omplexity_{o}f_{m}athematical_{o}per$

[26] J. Lin, N. Divekar, G. Lv, and R. D. Gregg, "Energy shaping control with virtual spring and damper for powered exoskeletons," in *IEEE Conf. Decis. Control*, 2019, pp. 3039–3045.

[27] H. K. Khalil, *Nonlinear systems*. Upper Saddle River, NJ: Prentice Hall, 2002, vol. 3.

[28] J. Lin, N. V. Divekar, G. Lv, and R. D. Gregg, "Optimal task-invariant energetic control for a knee-ankle exoskeleton," *IEEE Control Systems Letters*, 2020.

[29] R. Ortega, A. Van Der Schaft, B. Maschke, and G. Escobar, "Interconnection and damping assignment passivity-based control of port-controlled hamiltonian systems," *Automatica*, vol. 38, no. 4, pp. 585–596, 2002.

[30] R. Ortega, A. J. Van Der Schaft, I. Mareels, and B. Maschke, "Putting energy back in control," *IEEE Control Systems Magazine*, vol. 21, no. 2, pp. 18–33, 2001.

[31] N. Divekar, J. Lin, C. Nesler, S. Borboa, and R. D. Gregg, "A potential energy shaping controller with ground reaction force feedback for a multi-activity knee-ankle exoskeleton," in *IEEE Int. Conf. Biomed. Robot. Biomechatronics*, 2020.

[32] G. Morone, M. Matamala-Gomez, M. V. Sanchez-Vives, S. Paolucci,

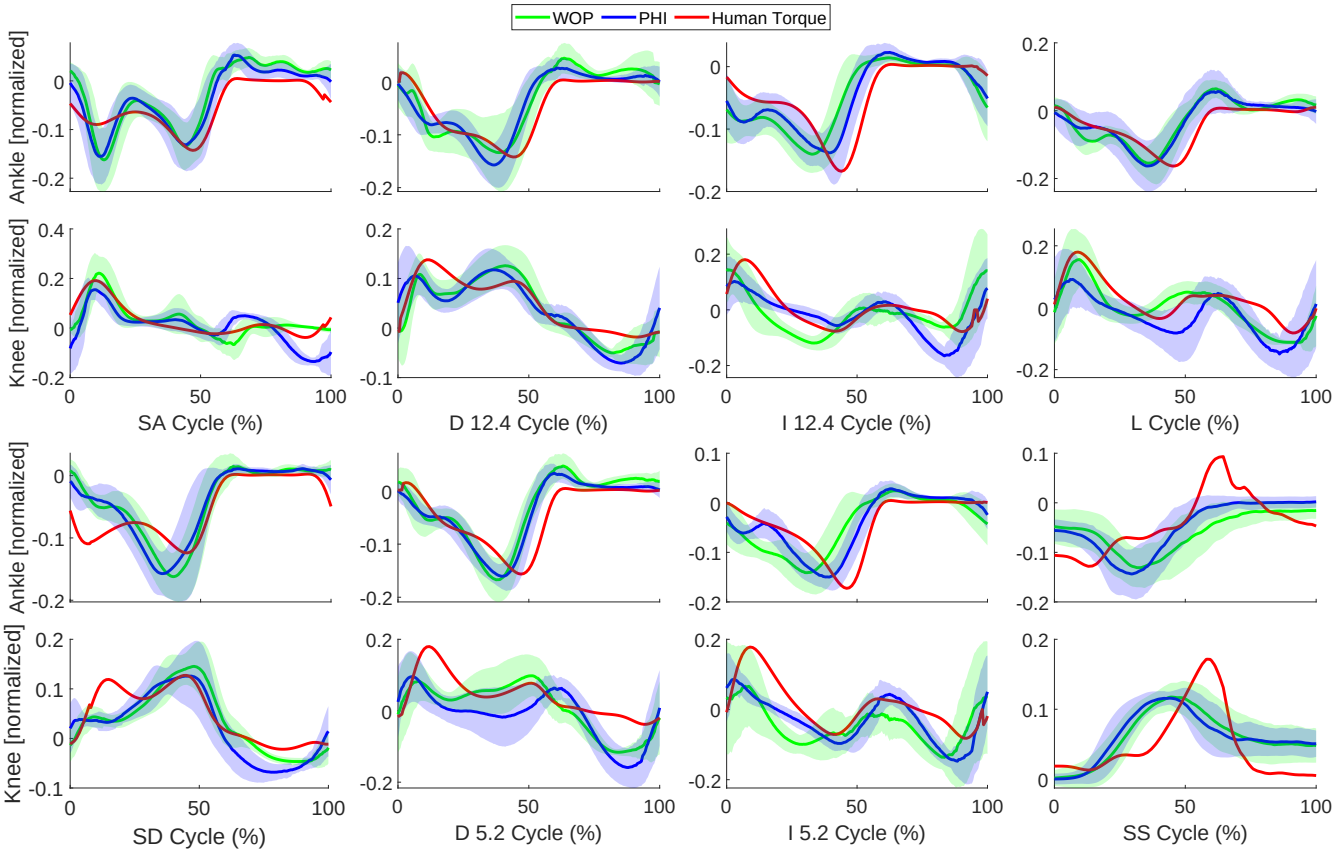

Fig. 7. Comparisons of across-subjects averaged command torques (PHI and WOP methods) and normative human torques for tasks {decline ($-5.2°, -12.4°$) and incline ($5.2°, 12.4°$), level ground (1 m/s), Stairs Ascent/Descent (7inch), Stand-to-Sit}. The blue solid (PHI method) and green solid (WOP method) lines represent the mean commanded exoskeleton torque (normalized by L2 normalization) across all repetitions for the active modes. The red solid line represents the normative human joint torques (normalized by L2 normalization) in [40], [41]. Positive torques represent ankle dorsiflexion and knee extension.

and M. Iosa, "Watch your step! who can recover stair climbing independence after stroke?" *Eur. J. Phys. Rehabil. Med.*, vol. 54, no. 6, p. 811—818, 2018.

[33] A. Boukadida, F. Piotte, P. Dehail, and S. Nadeau, "Determinants of sit-to-stand tasks in individuals with hemiparesis post stroke: a review," *Annals of physical and rehabilitation medicine*, vol. 58, no. 3, pp. 167–172, 2015.

[34] D. E. Chang, A. M. Bloch, N. E. Leonard, J. E. Marsden, and C. A. Woolsey, "The equivalence of controlled lagrangian and controlled hamiltonian systems," *ESAIM: Control, Optimisation and Calculus of Variations*, vol. 8, pp. 393–422, 2002.

[35] K. R. Embry, D. J. Villarreal, R. L. Macaluso, and R. D. Gregg, "Modeling the kinematics of human locomotion over continuously varying speeds and inclines," *IEEE transactions on neural systems and rehabilitation engineering*, vol. 26, no. 12, pp. 2342–2350, 2018.

[36] S. Boyd and L. Vandenberghe, *Convex optimization*. Cambridge university press, 2004.

[37] D. R. Guichard *et al.*, *Single and Multivariable Calculus*. David R. Guichard, 2020.

[38] M. D. Ardema, *Analytical dynamics: theory and applications*. Springer Science & Business Media, 2005.

[39] R. M. Murray, *A mathematical introduction to robotic manipulation*. CRC press, 2017.

[40] J. Camargo, A. Ramanathan, W. Flanagan, and A. Young, "A comprehensive, open-source dataset of lower limb biomechanics in multiple conditions of stairs, ramps, and level-ground ambulation and transitions," *Journal of Biomechanics*, vol. 119, p. 110320, 2021.

[41] B. Laschowski, R. S. Razavian, and J. McPhee, "Simulation of stand-to-sit biomechanics for design of lower-limb exoskeletons and prostheses with energy regeneration," *bioRxiv*, p. 801258, 2020.

[42] K. R. Embry, D. J. Villarreal, and R. D. Gregg, "A unified parameterization of human gait across ambulation modes," in *2016 38th Annual International Conference of the IEEE Engineering in Medicine and Biology Society (EMBC)*. IEEE, 2016, pp. 2179–2183.

[43] K. R. Embry and R. D. Gregg, "Analysis of continuously varying kinematics for prosthetic leg control applications," *IEEE Transactions on Neural Systems and Rehabilitation Engineering*, vol. 29, pp. 262–272, 2020.

[44] H. Zhu, J. Doan, C. Stence, G. Lv, T. Elery, and R. Gregg, "Design and validation of a torque dense, highly backdrivable powered knee-ankle orthosis," in *Robotics and Automation (ICRA), 2017 IEEE International Conference on*. IEEE, 2017, pp. 504–510.

[45] P. Weiss, P. Zenker, and E. Maehle, "Feed-forward friction and inertia compensation for improving backdrivability of motors," in *2012 12th International Conference on Control Automation Robotics & Vision (ICARCV)*. IEEE, 2012, pp. 288–293.

[46] S. Seok, A. Wang, M. Y. Chuah, D. J. Hyun, J. Lee, D. M. Otten, J. H. Lang, and S. Kim, "Design principles for energy-efficient legged locomotion and implementation on the mit cheetah robot," *Ieee/asme transactions on mechatronics*, vol. 20, no. 3, pp. 1117–1129, 2014.

[47] Tekscan, "http://www.tekscan.com/sites/default/files/resources/FLX-A401-G.pdfFlexiForce Standard Model A401," 2020.

[48] R. Bitter, T. Mohiuddin, and M. Nawrocki, *LabVIEW: Advanced programming techniques*. Crc Press, 2006.

[49] J. F. Yang and D. Winter, "Electromyographic amplitude normalization methods: improving their sensitivity as diagnostic tools in gait analysis." *Archives of physical medicine and rehabilitation*, vol. 65, no. 9, pp. 517–521, 1984.

[50] P. J. Millington, B. M. Myklebust, and G. M. Shambes, "Biomechanical analysis of the sit-to-stand motion in elderly persons," *Archives of Physical Medicine and Rehabilitation*, vol. 73, no. 7, pp. 609–617, 1992.

[51] M. K. MacLean and D. P. Ferris, "Human muscle activity and lower limb biomechanics of overground walking at varying levels of

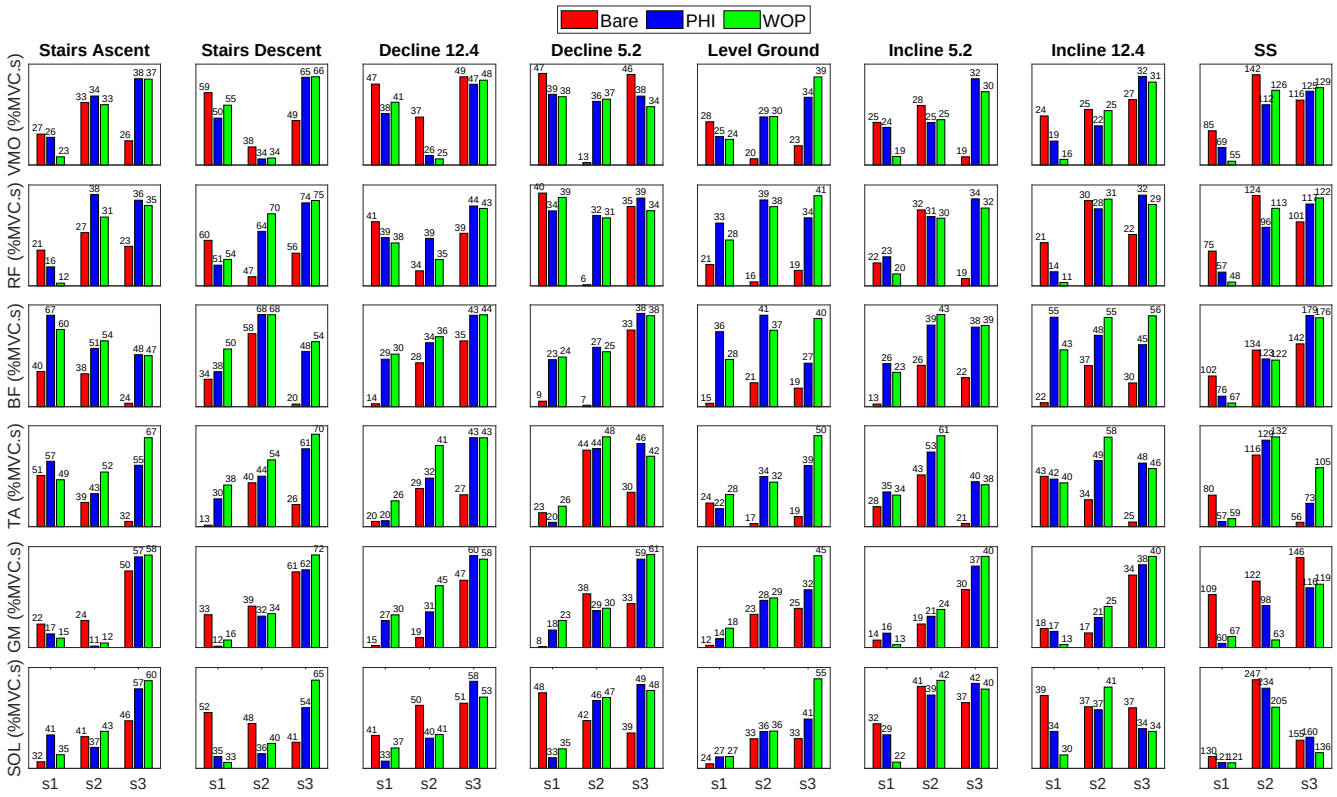

Fig. 8. Individual subject comparisons of mean effort across repetitions. Effort is compared between bare, active with PHI method, and active with WOP method for each muscle pair (VMO, RF, BF, TA, GM and SOL) and task and task {decline ($-5.2°, -12.4°$) and incline ($5.2°, 12.4°$) at 0.6 m/s, level ground (1 m/s for s1, s2, and s3, 0.85 m/s for s4, and 0.9 m/s for s5), Stairs Ascent/Descent (7in step height), and Sit-Stand cycle (45 BPM)}.

simulated reduced gravity and gait speeds," *PloS one*, vol. 16, no. 7, p. e0253467, 2021.

[52] T. Lenzi, M. C. Carrozza, and S. K. Agrawal, "Powered hip exoskeletons can reduce the user's hip and ankle muscle activations during walking," *IEEE Transactions on Neural Systems and Rehabilitation Engineering*, vol. 21, no. 6, pp. 938–948, 2013.